

Optimization of CFS sections under flexure using Genetic Algorithm

Optimización de secciones CFS bajo flexión usando el Algoritmo Genético

P.S. Kumar (*), G. Dhamodhara Kannan (**)

ABSTRACT

Economization of the structural systems by optimizing the elements is the recent trend receiving much attention in structural engineering designs. In this work, a numerical study is made to arrive at the optimal proportions of the cold-formed steel (CFS) Lipped C, Lipped Z, and Rectangular Hollow Flange sections (RHFB) when used as flexural members. Web depth to developed length ratio (k) and the flange width to lip depth ratio (a) are the two parameters taken for this optimization. Genetic algorithm was used to obtain the optimum values. Investigations are carried out on the variation in the moment capacity to the changes in dimensions of web, flange and lip. In this work developed length ranging from 100 mm to 500 mm and thickness of 1 mm to 3 mm were adopted. The moment capacity and buckling behavior of (CFS) sections are verified by non-linear finite element analysis using ABAQUS.

Keywords: Optimization; Rectangular hollow flange section; Genetic Algorithm; EuroCode 3.

RESUMEN

La tendencia actual en los diseños de la ingeniería estructural es el abaratamiento de los sistemas estructurales mediante la optimización de sus elementos. En este trabajo se emplean métodos numéricos para obtener las dimensiones óptimas de secciones conformadas en frío (CFS) tipo C, Z y en I con perfiles huecos rectangulares (RHFB) que se usan para piezas en flexión. Para la optimización se usaron dos parámetros, la relación entre la dimensión del alma y la longitud del desarrollo (k) y la relación entre la longitud del ala y la longitud del labio (a). Los valores óptimos se obtuvieron mediante algoritmos genéticos. Se investiga la variación del momento resistido con las variaciones en la dimensión del alma, el ala y el labio. Las longitudes de desarrollo consideradas en este trabajo van de 100 mm a 500 mm y los espesores adoptados desde 1 mm a 3 mm. El momento resistido y el comportamiento a pandeo de las secciones conformadas en frío (CFS) se verifican mediante el análisis por elementos finitos no lineales usando ABAQUS.

Palabras clave: Optimización; Sección conformada en I con perfiles huecos rectangulares; Algoritmo genético; Eurocódigo 3.

(*) Departamento de Ingeniería Civil, Profesor Asistente, Colegio de Tecnología del Gobierno, Coimbatore, (India).

(**) Departamento de Ingeniería Civil, Profesor, Facultad de Ingeniería de la Universidad, Ariyalur, Universidad de Anna

Persona de contacto/Corresponding author: kannan_civil@gct.ac.in (G. Dhamodhara kannan)

ORCID: <http://orcid.org/0000-0001-9108-5668> (P.S. Kumar); <https://orcid.org/0000-0001-6661-170X> (G. Dhamodhara Kannan)

Cómo citar este artículo/Citation: P.S. Kumar, G. Dhamodhara Kannan (2021). Optimization of CFS sections under flexure using Genetic Algorithm. *Informes de la Construcción*, 73(563): e399. <https://doi.org/10.3989/ic.76866>

Copyright: © 2021 CSIC. This is an open-access article distributed under the terms of the Creative Commons Attribution 4.0 International (CC BY 4.0) License.

Recibido/Received: 04/12/2019
Aceptado/Accepted: 05/10/2020
Publicado on-line/Published on-line: 15/09/2021

1. INTRODUCTION

In the design of any structural elements, adequate safety is to be guaranteed, and at the same time, it should be designed such that the cost is minimum. This is achieved by choosing the best geometry consistent with the functional requirements and proportioning the materials used for these structural elements in the most appropriate manner. In steel constructions, cold formed steel sections (CFS) are widely used. The modern CFS sections are quite complex, and they have a large number of independent parts. They are susceptible to different types of buckling and other constraints. Considerable scope exists in the rationalization and economization of CFS sections. In recent years this optimization receives much attention in the area of design. Engaging Genetic Algorithm, the symmetric CFS beam-column members are optimized by (1). Shape optimization of cold-formed thin-walled beams with an open cross section was carried out by (2). Investigation on variational and parametrical shaping of the prismatic beams in pure bending was carried out by (3). The shape optimization of CFS channel beams with 'drop' flanges (rounded return lips shaped like a water drop) was done by (4). Researchers have presented a thin-walled structure shape optimization methodology (5). An analytical and numerical elastic buckling study and a practical design of cold-formed thin-walled channel beams with various flange bend shapes under pure bending was carried out by (7). So far in the previous research works, only shape optimization was carried out. Size optimization on CFS sections are very limited. There is an indirect way of achieving cost reduction in construction by maximizing the usage of fabrication material. For example, for the given developed length and thickness, the proportioning of the lipped C section can be done in many possible ways as shown in figure 1. Though the weight of all sections is same, but its moment capacity will be different. Only one section among these proportion will have maximum capacity. Choosing the wrong one will lead to less capacity and necessitates the designer to go for bigger size sections. This will incur additional cost of construction and added weight to the structure. The aim in this work is to find the best among the possible proportions for achieving maximum capacity. By adopting the optimum proportion, utility of the material may be maximized and there is no further need to go for larger sections which in turn acquire further cost.

In this work, purlins in the roof system of a pre engineered steel structure is adopted for optimization. The design of a purlin has to withstand the moment arising from the combination of predominant loads like the dead, live, and wind loads. The nature of moment in a purlin may be of sagging or hogging depending upon the combination of wind load with other loads. The worst combination of loads will govern the design. In practice, the roof diaphragm connected to the compression flange of a purlin at a spacing not exceeding 300 mm through fasteners and it will act as a lateral restraint. During wind uplifting, the purlin is laterally unrestrained. To restrain the compression flange in case of wind uplift, it is a general practice to brace the bottom flange at suitable intervals with the top flange of adjacent purlins using sag rods. This bracing will act as a partial restraint and the portion of purlin between the bracings has to be designed for laterally unrestrained condition. In this study, the length between such bracing is taken as 2.5 m.

With the conditions given above, the aim of this work is to find the optimum proportion of the conventional lipped C, Z, and the newly formed Rectangular Hollow Flange sections (RHFB) for the given developed length. The RHFB sections has many advantages than the conventional sections due to tubular flanges. Research on the behaviour of the hollow flange channel beam under lateral buckling was carried out by researchers (6). The behaviour and capacity of light steel flexural members subject to Lateral Distortional Buckling was presented by (6). Experimental study on the section moment capacity of CFS beams with rectangular hollow flanges was carried out by (8).



Figure 1. Possible proportions of Lipped C section with a constant developed length

This work considers the advantage of flexibility in fabricating a CFS section in a local manufacturing unit. The CFS sections are optimized to achieve maximum bending and buckling resistance for the constant developed length. The shape of the CFS section is maintained, and only the dimensions are varied. Two dimensionless parameters were introduced namely the ratio of web depth to developed length (k) and flange width to lip depth ratio (a). In this work, size optimization was carried out to maximize the moment capacity for a given weight of material. This work can be used as a ready reckoner in the process of design of cold-formed steel sections. This helps in choosing the required developed length for the given moment and optimum dimensions of the CFS section for the chosen developed length.

2. GENETIC ALGORITHM

In the Engineering field, optimization techniques are introduced for solving technical problems. Conventional techniques are complicated in nature, and it is tough to solve. To overcome this difficulty, the Evolutionary optimization technique is used. Some of the prominent Evolutionary algorithms are hill-climbing, simulated annealing and the genetic algorithm. Genetic Algorithms (GAs) are trial and error search algorithms. It is based on Darwin's principle of natural selection. The facets are grouped as initial population, fitness function, selection, crossover, and mutation. It begins with randomly generated states. A bit string usually represents these states. For reproduction, two random pairs are selected. They are selected based on their fitness function score. For each pair to be mated, a cross over point is chosen at random from within the bit string. Exchanges between the parents actualize offspring

at the cross over point. The primary advantage of GA's comes from the cross over operation. Each location, in the bit string, can be subjected to a mutation with a small random probability. The fitness function generates the next generation of states, and it provides a score to each state. A proper fitness function should return to better states. GA is looking for a good and robust solution rated against Fitness criteria, so it avoids local optima and searches for global fitness. One may be selected more than once, whereas one may not be selected at all. The flow chart of GA is as shown in Figure 2. The population is diverse early in the process, causing the cross over to be maximum in the initial period. Nonetheless, in further generations, it will settle.

GA is used for generating high-quality solutions in optimization and search problems. Some of the popular applications are scheduling and sequencing, reliability design, vehicle routing and scheduling, group technology, facility layout, and location and transportation. In design field, GAs are used for finding an optimum cross-section of cold-formed steel beams, steel channels, lipped channel under axial compression. (29)

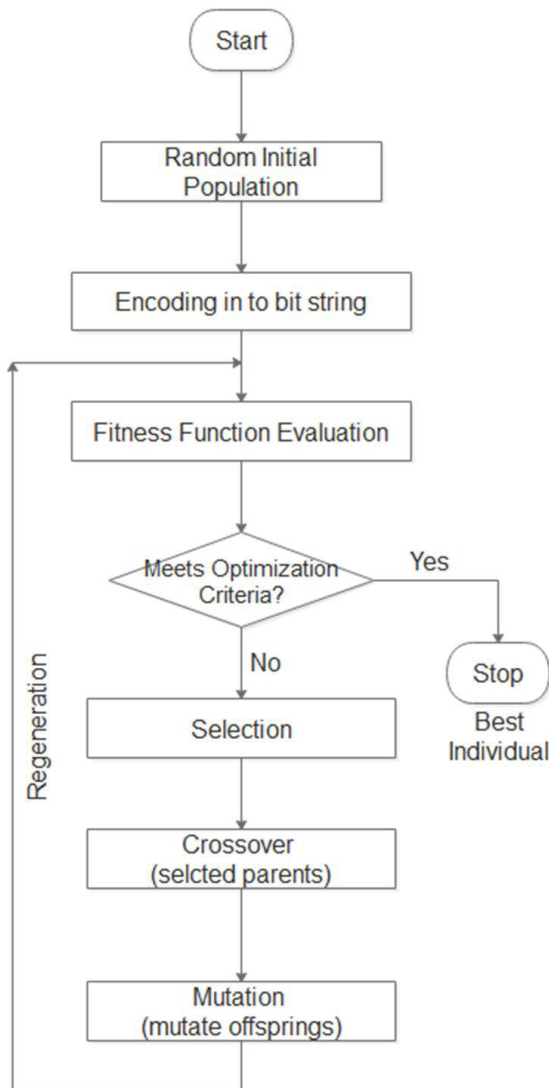


Figure 2. Flow chart for GA optimization

3. DESIGN OF CFS SECTION BASED ON EURO CODE 3

The objective of this optimization is to obtain an economical and efficient cross section dimensions for the given developed length and thickness. The Eurocode 3 predicts the design moment of CFS sections conservatively compared to other codes. The Euro code accounts for various buckling modes such as local, distortional, and lateral torsional buckling as shown in figure 4.

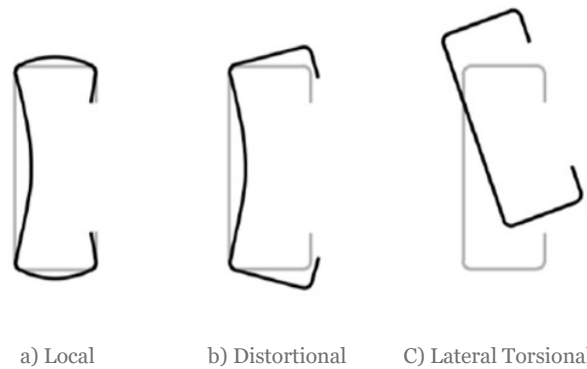
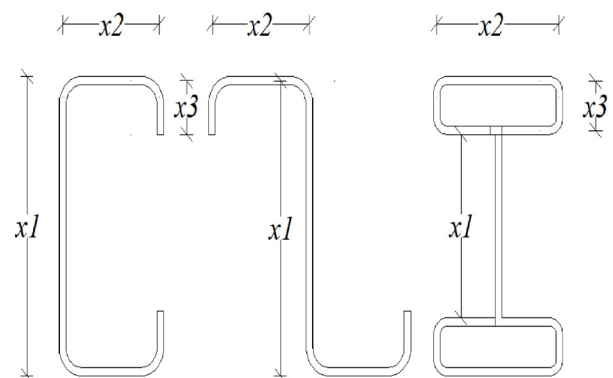


Figure 3. Local, Distortional and Lateral torsional buckling of a Lipped channel section.

Many researchers have investigated the buckling behavior of cold-formed steel channel section (9). The failure modes of local, distortional and global buckling, as well as yielding, in combination with deflection limits, were considered by (10). The problems of lateral buckling and local buckling of cold-formed steel beams in pure bending was addressed by (7). Researchers have used elastic buckling strength as an optimization criterion (11). ANNs have been applied to assess the effect of geometric parameters on Elastic Distortional Buckling Stress (12). The elastic behavior of hollow flange channel sections subject to uniform and non-uniform torsion, and combined torsion and bending was studied by (13). In this work, the provisions given in the EN1993-1-3 (EC3) has been taken for calculating the design bending moment of the CFS sections. The code considers the effective section properties of the compressed flange in calculating the bending and buckling resistance. Comparison on the stiffness of the experimental tests and finite element models engaging direct



x_1 : web depth, x_2 : Flange width, x_3 : lip depth

Figure 4. Design variables for Lipped C, Lipped Z and RHFB sections

strength and effective width method of predictions was done by (14). EC3 has following detailed provisions for the design of CFS members. Figure 3 presents the design variables.

3.1. Design for Local Buckling

Cold-formed steel sections usually have less thickness compared to hot rolled sections and easily susceptible to local buckling. Local buckling occurs within the element. Effective width concept uses uniform stress distribution in an equivalent width of the element to account for non-uniform stress distribution. Hence the buckled portion is omitted in the design moment calculations. The width of the buckled portion depends upon the plate slenderness, stress ratio, and yield strength of the plate. EC3 considers all the above parameters in calculating the effective portion of elements in the compression zone. The shift of the centroid due to reduced element width is also taken into account. Equations are given separately for stiffened and unstiffened elements. The stress level at which local buckling occurs is more than the stress level for distortional and lateral torsional buckling. Investigation on the global-local buckling behavior of thin-walled channel beams was carried out by (7). Works related to the structural behaviour and design of cold-formed lean duplex stainless steel (LDSS) hollow columns were done by (15). Local buckling occurs when the members have a shorter span. The plate slenderness equation is given by Equation [1]

$$[1] \quad \lambda_p = (bf/t) / (28.4 \varepsilon k\sigma)$$

Where $\varepsilon = \sqrt{(235/f_{yb})}$.

In Eq. [1] λ_p is the plate slenderness, bf is the breadth of the flange, t is the thickness, $k\sigma$ is the buckling factor, and in Eq. [2] f_{yb} is the basic yield strength.

3.2. Design for Distortional Buckling

Distortional buckling involves rotation of lip/flange about the flange/web junction. It induces due to local torsional buckling. In this case, the half wavelength of buckling is more than that of local buckling. This may occur in the support location also. This occurs due to insufficient stiffener in the compression zone. EC3 accounts for distortional buckling by reducing the effective thickness of stiffener elements in the compression zone. The stress level for distortional buckling to occur is more than that required for lateral torsional buckling and less than the stress in case of local buckling. This buckling occurs for members having an intermediate span. Studies on elastic lateral buckling of simply supported LiteSteel beams subject to transverse loading was addressed by (16).

The distortional slenderness is given by Equation [2]

$$[2] \quad \lambda_d = f_y / \sigma_{crs}$$

In Eq. [2] λ_d is the distortional slenderness, σ_{crs} is the elastic buckling stress of the plate stiffener assembly, f_y is the yield strength of the plate.

3.3. Design for Lateral Torsional Buckling

Lateral torsional buckling occurs for members which are in unrestrained condition. This condition occurs when the

compression flange is not supported throughout its length. This is usually observed in members having an open cross-section. LTB involves rotation of entire cross section with or without element buckling. Individual elements may undergo local or distortional buckling depending upon their participation factor with LTB. Design against LTB depends upon the effective length of the member, point of application of load, End support condition, moment gradient, and torsional stiffness of the section. The slenderness for lateral-torsional buckling λ_{LT}

$$[3] \quad \lambda_{LT} = \sqrt{W_{eff} \cdot f_y / M_{cr}}$$

where M_{cr} is the elastic lateral-torsional buckling moment, and W_{eff} is the effective section modulus.

4. OPTIMIZATION

Any system or component is described by a set of variables which influence the characteristics of the system. In- this optimization, for a given developed length and thickness, the variables identified are flange width, web depth and lip depth. To maintain the monosymmetry, dimensions of flange and lip were maintained same at top and bottom. This reduces the total number of variables. The flange width and lip depth are related by a parameter (a) as the ratio of flange width to lip depth, and thus, one of the variables is eliminated. The web depth to developed length ratio was taken as the other parameter (k). With these parameters as design variables, the moment carrying capacity is taken as the objective function. The constraints given in EC3 guidelines were incorporated in the form of limits of design variables as given in Table 1. The design variables which does not comply with the EC3 guidelines are eliminated as infeasible individuals.

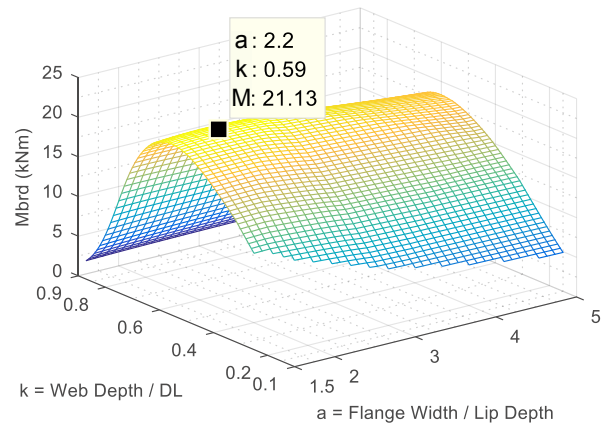
Table 1. Design Parameters and Constraints

Objective function	$M_{crd} = W_{eff} \cdot f_y / \gamma$, For laterally restrained condition $M_{brd} = \chi_{LT} \cdot W_{eff} \cdot f_y / \gamma$, For laterally unrestrained condition. χ_{LT} – reduction factor for lateral torsional buckling.
Geometrical constraints	$0 < x_1, x_2, x_3 < DL$ $x_1 + x_2 + x_3 = DL$ $2 x_3 \leq x_1$
EC3 constraints	$x_1/t \leq 500$ $x_2/t \leq 60$ $x_3/t \leq 50$ $0.2 \leq x_3/x_2 \leq 0.6$
Design variables	$k = x_1 / DL$ $a = x_2 / x_3$
Upper and Lower limits of design parameters	$0.1 \leq k \leq 0.9$ $1.6 \leq a \leq 5$
Expression for arriving dimensions of CFS	$x_1 = k \cdot DL$ $x_2 = a \cdot x_3$ $x_3 = DL(1-k) / (1+a)$
Constants	Developed Length (DL) and thickness (t)
Parameters in Genetic algorithm setup	Lower bounds of search space - [0.1 , 1.6] Upper bounds of search space - [0.9, 5] Population size - 100 Maximum number of generations - 50 Mutation probability - 0.1 Crossover rate – 0.8 Migration Interval - 20

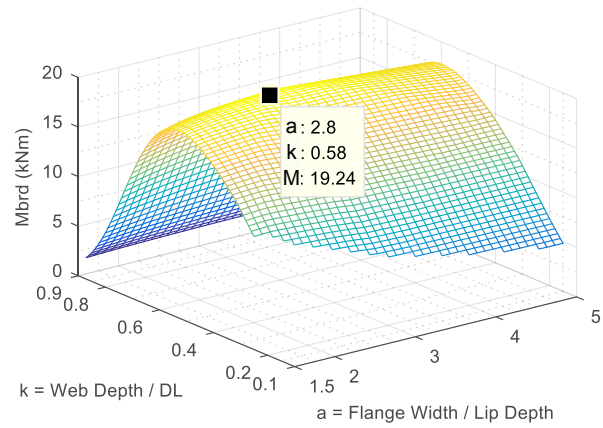
Hence in this optimization problem, only two non dimensional parameters are defined, and all the profile dimensions can be calculated from these parameters. The limits of Design variables are obtained to satisfy the limiting value of flat width to thickness ratios as laid down by the EC3 and the geometrical constraints as given in the Table 1. 3D plots of moment capacity was plotted for all possible values of these parameters and plotted as shown in (Figure 5-7) using MATLAB for better understanding. This 3D plot depicts the optimum design values for maximum moment capacity for a constant developed length of 500mm and thickness of 2mm. This ensures the same weight of all sections and better relative comparison. Symbolic calculations to find the design moment for the given values of design parameters were scripted in MATLAB. The genetic algorithm was used to find the optimum values for all the developed length ranging from 100 mm to 500mm and thickness from 1mm to 3mm. The parameters in genetic algorithm setup is given in Table 1. Initially, the population is formed by randomly selecting the design parameters within the range. Each candidate in the initial population is converted into binary form. After decoding, these individuals that represent the proportions are used to calculate dimensions of the CFS section and its moment capacity as per EC3. In the next iteration, the fittest individuals obtained from the previous generation are subjected to GA operations such as selecting the best individual, cross over, and mutation. This process of GA technique is continued until the maximum value of objective function is reached.

4.1. Discussion of the results

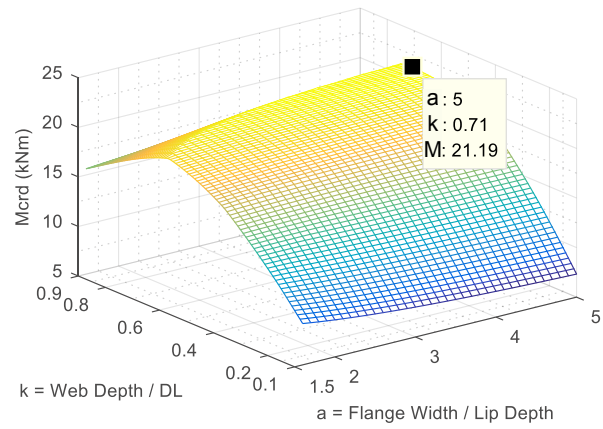
From Figure 5, 3D contour plots show the variation of design bending moment with various values of design parameters (k) and (a) for all CFS sections. The design parameters were varied within limits specified in the EC3 and from practical considerations. Among the possible combinations of design parameters, the section which gives maximum M_{brd} or M_{crd} is optimum. At lower and upper values of design parameters, the design bending moment is low compared to their intermediate values. As these parameters increase, the design bending moment also increases and reaches maximum and then decreases.



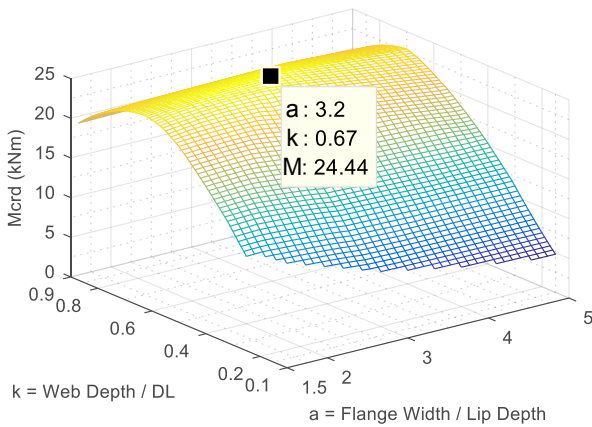
b) Lipped 'C' Section (M_{brd})



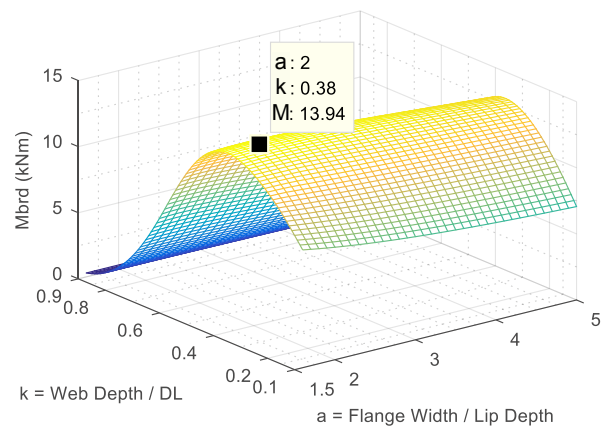
c) Lipped 'Z' Section (M_{brd})



d) RHFB Section (M_{crd})



a) Lipped 'C' & 'Z' Section (M_{crd})



e) RHFB Section (M_{brd})

Figure 5. 3D Contour plot of design moment for various (k) & (a) parameters

4.2. Effect of the parameter (k) on the design bending moment

The graph between design moment and design parameter (k) is plotted as shown in Figure 6. There is a quickly increasing trend in the values of M_{crd} or M_{brd} as the design parameter (k) increases and reaches the maximum, and then there is a decreasing trend. The design parameter (k) has a narrow zone of optimum values. This indicates the (k) ratio greatly influences in the design bending moment compared to other parameters. The design parameter (k) value more or less than the optimum has a significant influence on the design bending moment of CFS sections. A lower value of (k) results in lesser depth, which provides insufficient stiffness in the plane of bending. A higher value of (k) ratio gives more depth but deficient in its lateral strength leading to lateral torsional buckling. The choice of depth of the section should be such that it has maximum stiffness in the plane of bending as well as it has to satisfy the adequate lateral stiffness to resist the lateral torsional buckling.

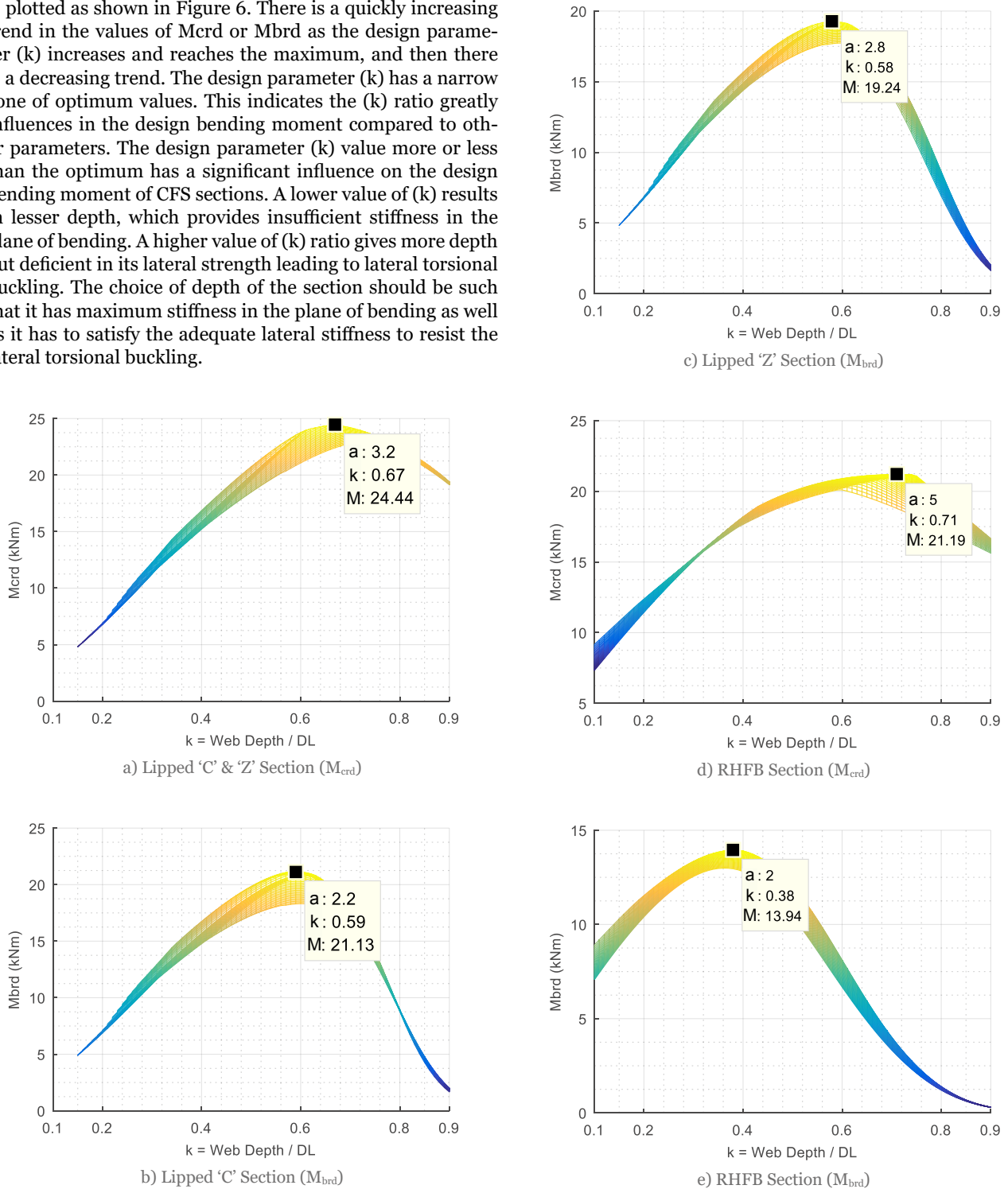


Figure 6. Variation of design moment for various values of the parameter (k)

4.3. Effect of the parameter (a) on the design bending moment

The effect of (a) ratio as shown in (Figure 7) has more influence on the design bending moment until it reaches a value of 1. After that, the (a) parameter does not have any significant effect on the design bending moment. A higher value of the parameter (a) results in less lip depth, which is an insufficient and wider flange, which is susceptible to local buckling. A lower value of the parameter (a) results in a deeper lip, which is an ineffective and narrow flange, which gives less lateral buckling strength. It is observed that the parameter (a) has a broader zone of optimum values than (k) parameter, which gives the flexibility of choosing more values without significant change in the maximum design bending moment. The optimum value of parameter (a) has reached upper limit for RHFB section.

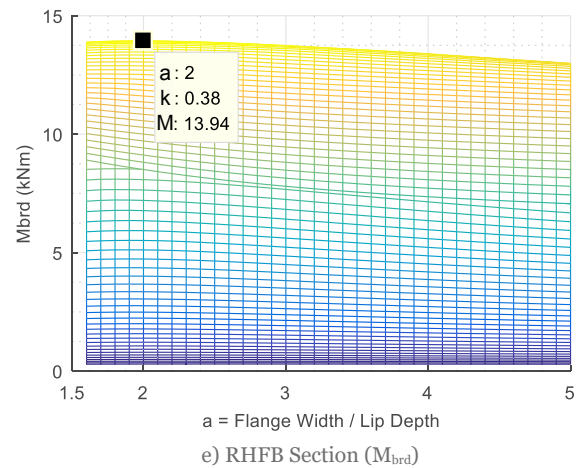
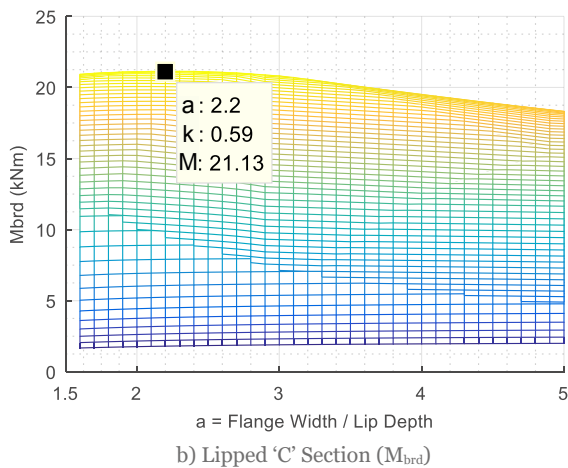
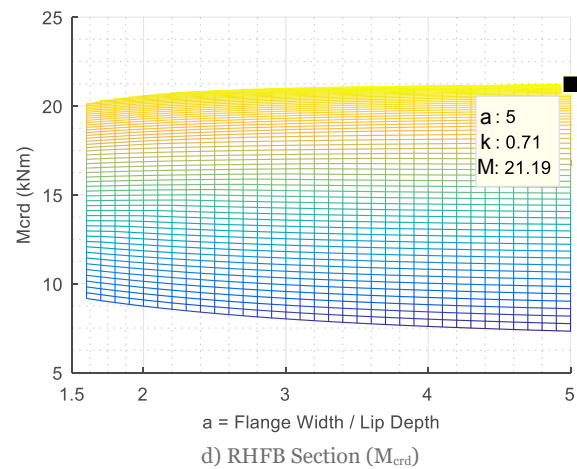
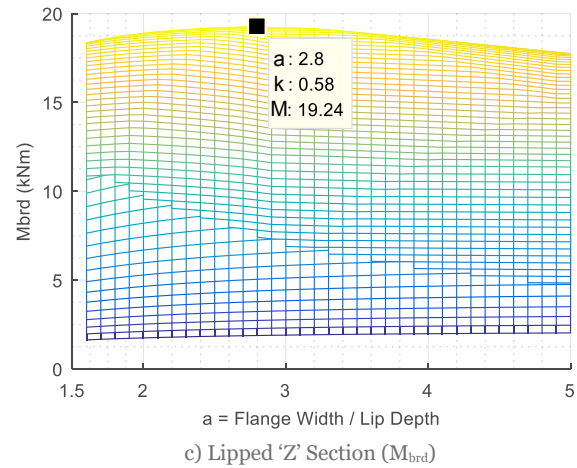
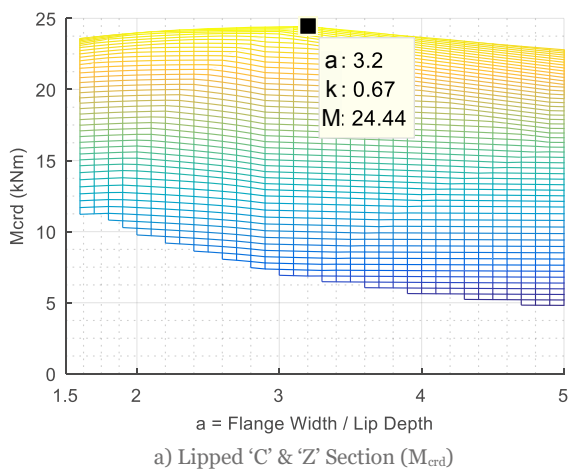


Figure 7. Variation of design moment for various values of the parameter (a)

4.4. Design moment for various developed lengths

The maximum design bending moment of CFS sections obtained from possible proportions using a genetic algorithm is plotted against various values of developed length as shown in Figure 8. The results indicate that the design bending moment increases with the increase in developed length and thickness if corresponding optimum proportions are adopted for fabricating the CFS sections. This graph can

be used for selecting the minimum developed length required to attain the design moment capacity in the process of design.

5. FINITE ELEMENT ANALYSIS

Finite element analysis (FEA) was carried out using ABAQUS to simulate the flexural behavior of CFS sections as shown in Figure 10 (a,b,c,d). FEA provides an inexpensive and time efficient alternative to a physical test.

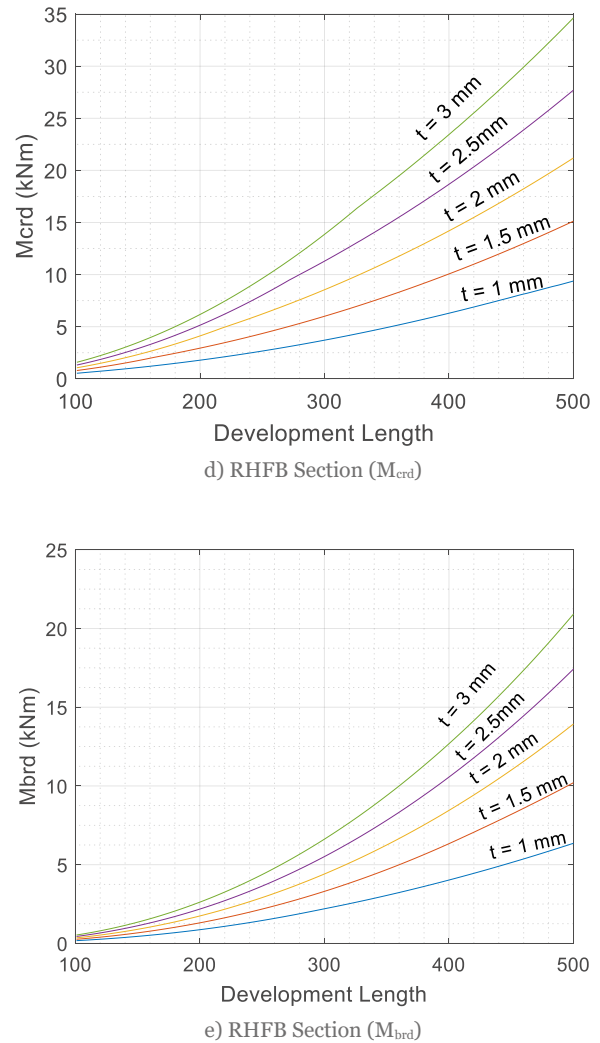
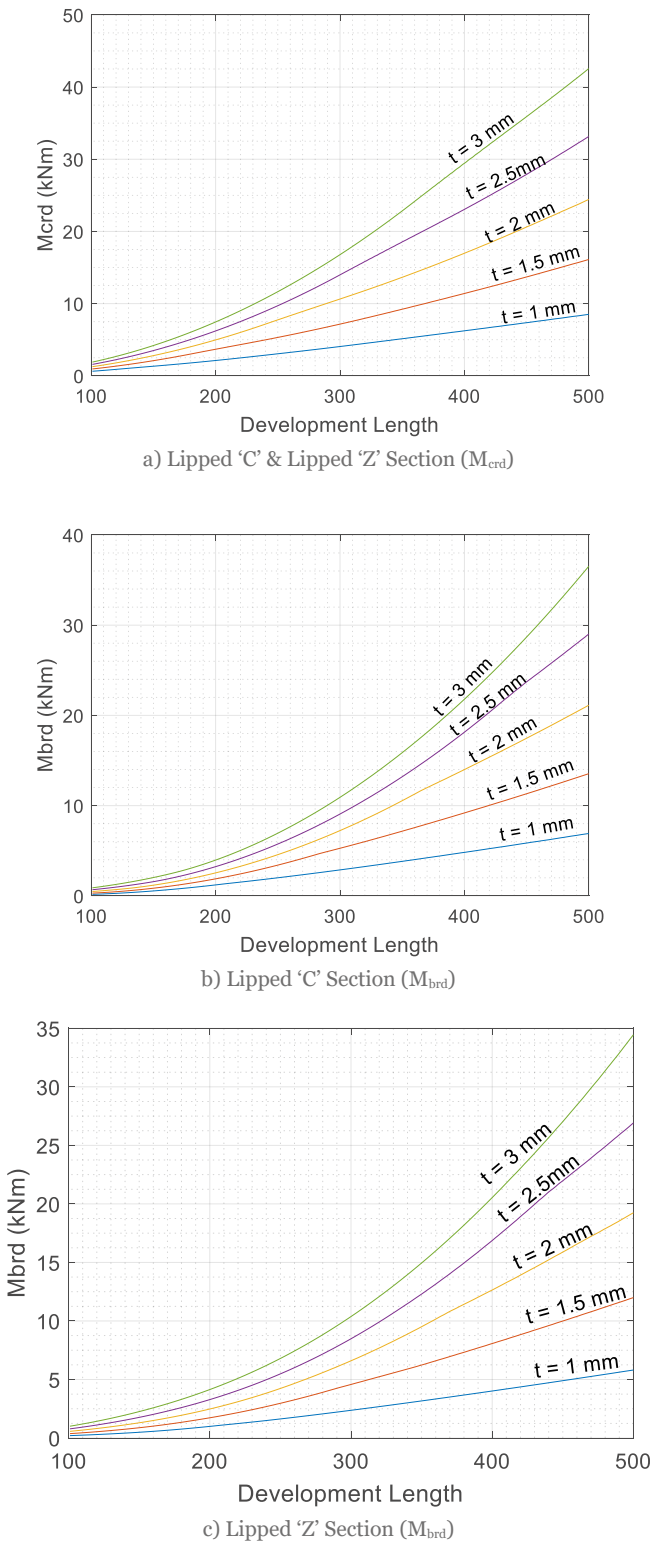


Figure 8. Variation of design moment with Developed Length (DL)

The flexural behaviour and buckling modes of optimized CFS sections were studied. The reserve capacity of optimized CFS section available more than the predicted capacity by EC3 was investigated. The detailed geometric and material non-linear model was used in this study. In each CFS section, fifteen models with various developed length, thickness, and optimized design parameters were used. FEA has become an essential tool in any CFS related research work. Numerical study on the section moment capacity of a doubly symmetric hollow flange steel plate girder (HFSPG) for use in long span applications was carried out by (17). The deformation of rectangular tubes in bending was investigated using the finite element method. Many researchers have evaluated the rotation capacity of cold-formed steel (CFS) beams through numerical investigation (18,19). Parametric study was carried out and new design equations for the section moment capacity of RHFCBs in the Direct Strength Method was proposed by (20).

5.1. Finite Element Modelling

Lipped C, Lipped Z, and Rectangular hollow flange CFS sections have been considered for this numerical analysis. All the sections were subjected to constant end moments in this numerical study. Unsupported length of the section was taken as 2500 mm. The thickness of 1 mm, 1.5 mm, 2 mm,

2.5 mm, and 3 mm have been taken into this study. Cross section dimensions of the CFS sections modeled in the finite element analysis are presented in Table 2. Finite element models of CFS sections were developed in ABAQUS using the general purpose S4R shell element. This element is a four-noded quadrilateral shell element with reduced integration. It is common practice to use shell element in order to model buckling problems. A mesh size of 10 mm with an aspect ratio of not less than one was used for meshing the model. Numerous previous research studies have demonstrated that this element can model plate buckling problems with excellent accuracy and have shown excellent comparisons with experimental results (21,22,23,27).

5.2. Material model

For the preliminary investigation, cold-formed steel having yield stress of 350 N/mm² is considered in this study. Initially, a buckling analysis was carried out with elastic properties of standard steel. Elastic modulus and Poisson's ratio were taken as 210 GPa and 0.3, respectively. The most realistic hardening behaviour of the material is required to simulate the post-buckling behaviour of members. For Non-linear analysis, a bilinear model having linear stress-strain relation up to 0.2% proof stress, followed by a straight line with a constant slope of E/100 was adopted as recommended in Eurocode 3 part 1-5. This model is similar to the elastic-perfect plastic model. In this study, the perfect plastic model was adopted after the elastic range since the strains at the maximum moment are less than the strains in the post-buckling stage.

5.3. Boundary Conditions and loading

The cross-section profile is developed in the XY plane and extruded along the Z-axis in the finite element model. The nodal displacements are referred to as (U1, U2, U3) and rotations as (UR1, UR2, UR3) in global X, Y and Z axis, respectively. The simply supported end conditions were modeled as shown in figure 9. The reference point was inserted at the

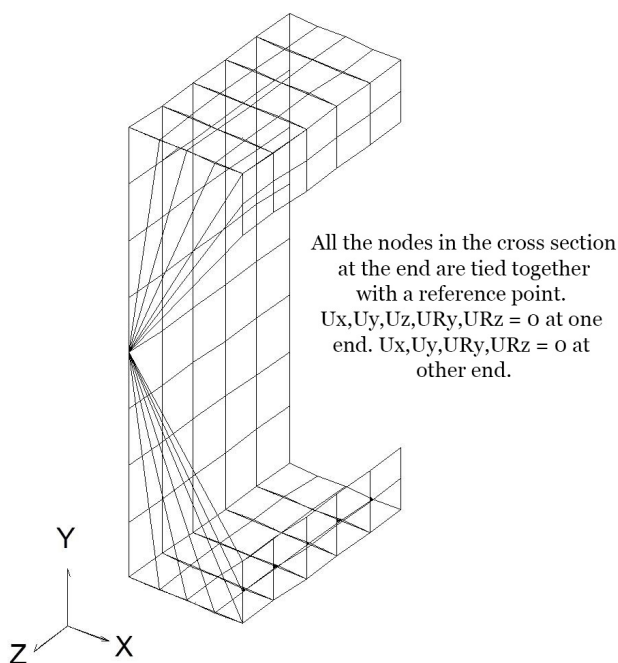


Figure 9. Boundary Condition in FEM model

middle of the web at the end of the beam. All the nodes lying in the cross-section at the end of the beam were tied to this reference point. This ensures rotation of the cross-section plane along with the reference point. Since the reference point and set of nodes in the plane of the cross-section at the ends tied, the applied moment is distributed along the end section. Free warping of flange nodes is permitted at the ends. Hinged boundary condition at one end and roller boundary condition at the other end was introduced. A concentrated moment of unit magnitude about the bending axis is applied for buckle analysis. The critical moment obtained from the buckling analysis was applied at the ends in the non-linear analysis.

5.4. Analysis

In this study, buckle analysis on the perfect model and geometrically and Materially Nonlinear Analysis on imperfection models (GMNIA) (24). Initially, a linear buckle analysis was performed in order to obtain elastic critical moment and various buckling modes. A node file consists of nodal coordinate data, and corresponding displacements from all the buckling modes is generated by editing the ABAQUS keyword file of the model. As mentioned by (25) that it is rational not to incorporate the residual stresses into the finite element models explicitly; an equivalent geometric imperfection is given. The nodal displacement in linear buckle analysis scaled to span/200 and incorporated in the ideal model as local imperfection for non-linear analysis (24). This local imperfection also accounts for residual stresses induced due to cold forming operation. In combining imperfection, the primary mode was given full weightage while the values of accompanying mode reduced to 70%. In addition to local imperfection, a global imperfection of span/1000 was given for the finite element model developed for calculating design buckling resistance (M_{brd}). Riks method of non-linear analysis has been carried for this imperfection model. The initial increment was given as 0.01. The maximum number of iterations was given as 50, which are required for obtaining a force-displacement relationship in the post-buckling region. In the Riks analysis, the failure criterion used for the numerical study is the one recommended in Eurocode 3 part 1-5, for structures susceptible to buckling, i.e., as the point at which the maximum value of the moment is obtained. Thus the present analysis has been performed by employing the Riks algorithm, well known for being used in conjunction with stability problems.

5.5. Comparison of results of genetic algorithm and FEA

The primary and secondary buckling modes and the corresponding critical moment are compared for these sections. It is evident that section 2 with intermediate web depth resists more significant moment compared with the shorter or deeper web. The buckling modes of these sections also compared. Section 1 with deeper web lacks in lateral torsional resistance. Section 3 with shorter web though resists lateral torsional buckling in a better way but its in-plane bending capacity is less, and compression flange suffers from local buckling. The results of optimization using a genetic algorithm for CFS sections are presented in Table 2. The moment capacity for optimum profiles from EC3 is compared with the results obtained from finite element analysis. It can be noticed from Table 2 that the width requirement of the flange increases with an in-

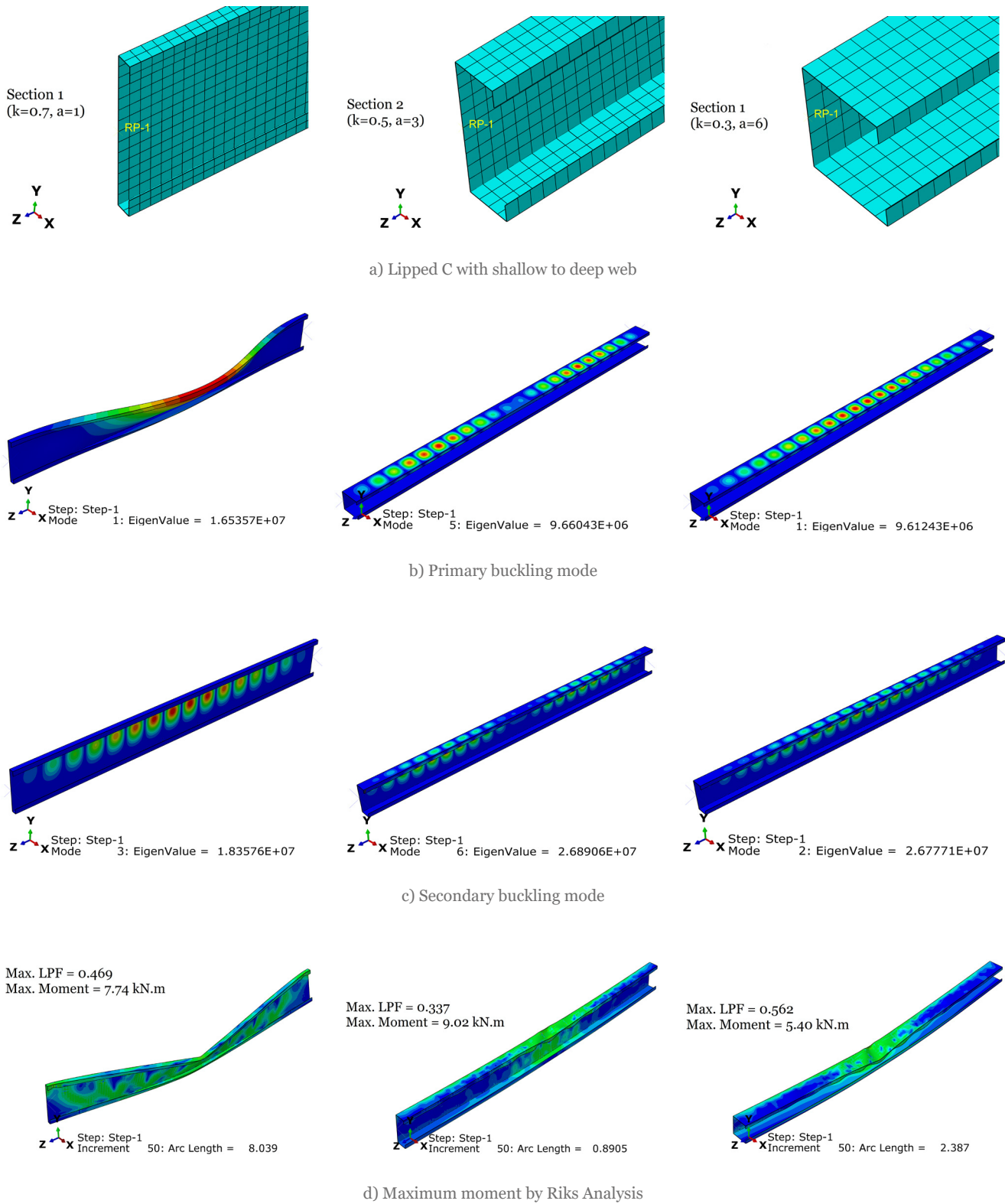


Figure 10 Comparison of the behavior of Lipped 'C' Sections with different design parameters.

Table 2. Dimensions of the CFS sections and comparison between EC3 - FEA

DL (mm)	k	a	t (mm)	dw (mm)	bf (mm)	df (mm)	M _{crd} (kN m)			M _{brd} (kN m)		
							EC 3	FEA	FEA/EC3	EC 3	FEA	FEA/EC3
Lipped C Section												
200	0.44	1.7	1	88	35	21	1.67	1.72	1.03	1.28	1.31	1.02
200	0.42	2	1.5	84	39	19	2.54	3.02	1.19	1.93	2.21	1.14
200	0.43	2.1	2	86	39	18	3.49	4.04	1.16	2.59	3.03	1.17
200	0.43	2.3	2.5	86	40	17	4.41	5.19	1.18	3.27	3.92	1.20
200	0.44	2.5	3	88	40	16	5.44	6.78	1.25	3.97	4.84	1.22
300	0.54	1.6	1	162	42	27	3.48	3.56	1.02	2.86	3.01	1.05
300	0.5	2	1.5	150	50	25	6.38	6.85	1.07	4.96	5.62	1.13
300	0.5	2.3	2	150	52	23	8.9	9.11	1.02	6.62	8.02	1.21
300	0.5	2.3	2.5	150	52	23	11.13	12.31	1.11	8.29	10.23	1.23
300	0.5	2.4	3	150	53	22	13.41	15.35	1.14	9.97	12.54	1.26
400	0.61	1.3	1	244	44	34	5.55	6.11	1.10	4.61	5.27	1.14
400	0.57	1.8	1.5	228	55	31	10.52	11.23	1.07	8.51	9.53	1.12
400	0.54	2.2	2	216	63	29	15.97	16.88	1.06	12.47	12.70	1.02
400	0.55	2.4	2.5	220	64	26	21.17	23.54	1.11	15.71	17.58	1.12
400	0.55	2.5	3	220	64	26	25.48	27.65	1.09	18.87	21.72	1.15
Lipped Z Section												
200	0.42	3.7	1	84	46	12	1.67	1.70	1.02	0.99	1.35	1.36
200	0.41	4.9	1.5	82	49	10	2.54	2.65	1.04	1.73	1.95	1.13
200	0.41	5	2	82	49	10	3.49	3.78	1.08	2.48	2.66	1.07
200	0.43	5	2.5	86	48	10	4.41	5.00	1.13	3.28	3.56	1.08
200	0.45	5	3	90	46	9	5.44	6.28	1.15	4.14	4.54	1.10
300	0.51	2.1	1	153	50	24	3.48	3.65	1.05	2.37	2.74	1.16
300	0.48	3.4	1.5	144	60	18	6.38	6.78	1.06	4.58	5.26	1.15
300	0.48	4.5	2	144	64	14	8.9	9.67	1.09	6.6	7.68	1.16
300	0.48	5	2.5	144	65	13	11.13	12.50	1.12	8.48	9.32	1.10
300	0.48	5	3	144	65	13	13.41	15.20	1.13	10.38	12.22	1.18
400	0.58	1.6	1	232	52	32	5.55	5.88	1.06	4.02	5.04	1.25
400	0.55	2.4	1.5	220	64	26	10.52	10.95	1.04	8.07	8.72	1.08
400	0.53	3.5	2	212	73	21	15.97	16.74	1.05	12.64	15.15	1.20
400	0.52	4.3	2.5	208	78	18	21.17	22.80	1.08	16.87	17.2	1.02
400	0.52	5	3	208	80	16	25.48	28.63	1.12	20.54	22.85	1.11
Rectangular Hollow Flange Section												
200	0.28	1.7	1	56	23	13	1.18	1.32	1.12	0.87	1.00	1.15
200	0.28	1.7	1.5	56	23	13	1.77	1.82	1.03	1.31	1.58	1.21
200	0.28	1.7	2	56	23	13	2.37	2.65	1.12	1.74	1.97	1.13
200	0.28	1.7	2.5	56	23	13	2.96	3.11	1.05	2.18	2.68	1.23
200	0.28	1.7	3	56	23	13	3.55	3.84	1.08	2.62	2.99	1.14
300	0.32	1.6	1	96	31	20	2.84	2.95	1.04	2.2	2.26	1.03
300	0.32	1.8	1.5	96	33	18	4.27	4.82	1.13	3.3	3.8	1.15
300	0.32	1.8	2	96	33	18	5.7	6.1	1.07	4.41	5.16	1.17
300	0.32	1.8	2.5	96	33	18	7.12	7.53	1.06	5.51	6.73	1.22
300	0.33	1.8	3	99	32	18	8.69	8.87	1.02	6.62	8.27	1.25
400	0.36	1.6	1	144	39	25	5.06	5.32	1.05	4.02	4.35	1.08
400	0.36	1.9	1.5	144	42	22	8.09	8.86	1.09	6.33	7.28	1.15
400	0.36	1.9	2	144	42	22	10.79	12.28	1.14	8.45	9.21	1.09
400	0.36	1.9	2.5	144	42	22	13.49	14.95	1.11	10.56	11.62	1.10
400	0.36	1.9	3	144	42	22	16.19	17.12	1.06	12.68	15.22	1.20

Table 3. Optimum Design parameters for various developed lengths

DL (mm)	dw/DL					bf/df					
	t →	1	1.5	2	2.5	3	1	1.5	2	2.5	3
Lipped C & Z Section- M_{crd}											
100	0.81	0.81	0.81	0.81	0.81	5.0	5.0	5.0	5.0	5.0	5.0
200	0.63	0.73	0.81	0.81	0.81	3.8	5.0	5.0	5.0	5.0	5.0
300	0.69	0.63	0.65	0.81	0.81	2.7	3.8	5.0	5.0	5.0	5.0
400	0.76	0.68	0.63	0.66	0.73	2.2	3	3.8	4.8	5.0	5.0
500	0.79	0.71	0.67	0.63	0.65	1.7	2.4	3.2	3.8	4.6	4.6
Lipped C Section- M_{brd}											
100	0.31	0.35	0.37	0.4	0.42	1.9	5.0	5.0	5.0	5.0	5.0
200	0.44	0.42	0.43	0.43	0.44	1.7	2.0	2.1	2.3	2.5	2.5
300	0.54	0.5	0.5	0.5	0.5	1.6	2.0	2.3	2.3	2.4	2.4
400	0.61	0.57	0.54	0.55	0.55	1.3	1.8	2.2	2.4	2.5	2.5
500	0.66	0.62	0.59	0.56	0.57	1.6	1.7	2.3	2.5	2.8	2.8
Lipped Z Section- M_{brd}											
100	0.30	0.35	0.38	0.41	0.43	5.0	5.0	5.0	5.0	5.0	5.0
200	0.42	0.41	0.41	0.43	0.45	3.7	4.9	5.0	5.0	5.0	5.0
300	0.51	0.48	0.48	0.48	0.48	2.1	3.4	4.5	5.0	5.0	5.0
400	0.58	0.55	0.53	0.52	0.52	1.6	2.4	3.5	4.3	5.0	5.0
500	0.63	0.60	0.58	0.55	0.56	1.6	1.8	2.8	3.5	4.3	4.3
RHFB- M_{crd}											
100	0.90	0.90	0.90	0.90	0.90	1.6	1.6	1.6	1.6	1.6	1.6
200	0.76	0.89	0.90	0.90	0.90	5.0	5.0	1.6	1.6	1.6	1.6
300	0.68	0.76	0.86	0.90	0.90	5.0	5.0	5.0	5.0	5.0	1.6
400	0.64	0.70	0.76	0.84	0.89	5.0	5.0	5.0	5.0	5.0	5.0
500	0.65	0.67	0.71	0.77	0.83	5.0	5.0	5.0	5.0	5.0	5.0
RHFB- M_{brd}											
100	0.20	0.20	0.20	0.20	0.20	1.6	1.6	1.6	1.6	1.6	1.6
200	0.28	0.28	0.28	0.28	0.28	1.7	1.7	1.7	1.7	1.7	1.7
300	0.32	0.32	0.32	0.32	0.33	1.6	1.8	1.8	1.8	1.8	1.8
400	0.36	0.36	0.36	0.36	0.36	1.6	1.9	1.9	1.9	1.9	1.9
500	0.38	0.38	0.38	0.38	0.38	1.7	1.7	2.0	2.0	2.0	2.0

crease in the thickness. This implies that the lateral bending resistance required in the compression flange is more significant for the thicker web to carry higher in-plane moment. A flange width less than the optimum is insufficient, and more than the optimum is ineffective to restrain the web from lateral buckling. It is also seen that the lip depth requirement decreases as the thickness of the section increases. For instance, the lip depth required for 1 mm thickness of lipped C section is 34 mm as against 26 mm for 3 mm thickness for a developed length of 400 mm. This trend indicates that as the thickness of the lip portion increases, it requires less depth for stiffening the compression flange. A lip depth less than the optimum have insufficient stiffness, and more than the optimum is not effective in stiffening the flange. EC3 is conservative in predicting the moment capacity of lipped C, lipped Z and RHFB sections, but it is slightly over-conserv-

ative for larger values of developed length and thicker CFS sections. The developed length and thickness required to resist the given bending moment is provided in Table 3 for reference. After deciding the preliminary proportion, its moment capacity has to be verified against the required moment capacity as this is mandatory in the design process.

6. CONCLUSION

In this attempt, an approach engaged a genetic algorithm for finding the optimum dimensions of cold-formed steel sections for an economical construction. The minimum requirement of developed length and thickness to resist the given bending moment is given. The optimum proportions for both laterally restrained and laterally unrestrained condition are separately investigated for various developed length and

thickness. For other values of developed length, linear interpolation can be adopted. The variation in the design moment capacity due to linear interpolation for intermediate values was investigated, and it is found to be a maximum of only 5% in limited cases. All the optimum value of design parameters are within the constraints given in EC3 except for RHFB. Finite element analysis has been carried out for 45 CFS sections and compared with the design moment obtained from EC3. In future, the upper limit of parameter (a) for RHFB sections may be increased beyond the EC3 constraints to identify any improvement in the moment capacity in laterally restrained

condition. This investigation indicates that there is a need to search for other practical profiles to improve the buckling resistance for the given developed length.

ACKNOWLEDGEMENTS

The author is grateful to the Government College of Technology, Coimbatore, for providing a licensed version of ABAQUS under TEQIP-II for the above work. The author is also thankful to the college for providing access to Scopus indexed journals under TEQIP II.

REFERENCES

- (1) Parastesh, H., Hajirasouliha, I., Taji, H., & Bagheri Sabbagh, A. (2019). Shape optimization of cold-formed steel beam-columns with practical and manufacturing constraints. *Journal of Constructional Steel Research*, 155, 249–259. <https://doi.org/10.1016/j.jcsr.2018.12.031>.
- (2) Karim, A., & Adeli, H. (2000). Global Optimum Design of Cold-Formed Steel I-Shape Beams. *Practice Periodical on Structural Design and Construction*, 5(2), 78–81. [https://doi.org/10.1061/\(ASCE\)1084-0680\(2000\)5:2\(78\)](https://doi.org/10.1061/(ASCE)1084-0680(2000)5:2(78)).
- (3) Magnucki, K., & Magnucka-Blandzi, E. (1999). Variational design of open cross-section thin-walled beam under stability constraints. *Thin-Walled Structures*, 35(3), 185–191. [https://doi.org/10.1016/S0263-8231\(99\)00031-2](https://doi.org/10.1016/S0263-8231(99)00031-2).
- (4) Magnucki, K., & Paczos, P. (2009). Theoretical shape optimization of cold-formed thin-walled channel beams with drop flanges in pure bending. *Journal of Constructional Steel Research*, 65(8–9), 1731–1737. <https://doi.org/10.1016/j.jcsr.2009.03.010>.
- (5) Vinot, P., Cogan, S., & Piranda, J. (2001). Shape optimization of thin-walled beam-like structures. [https://doi.org/10.1016/S0263-8231\(01\)00024-6](https://doi.org/10.1016/S0263-8231(01)00024-6).
- (6) Anapayan, T., Mahendran, M., & Mahaarachchi, D. (2011). Lateral distortional buckling tests of a new hollow flange channel beam. *Thin-Walled Structures*, 49(1), 13–25. <https://doi.org/10.1016/j.tws.2010.08.003>.
- (7) Magnucka-Blandzi, E., & Magnucki, K. (2011). Buckling and optimal design of cold-formed thin-walled beams: Review of selected problems. *Thin-Walled Structures*, 49(5), 554–561. <https://doi.org/10.1016/j.tws.2010.09.011>.
- (8) K.S. Wanniarachchi, M. Mahendran, Experimental study of the section moment capacity of cold-formed and screw-fastened rectangular hollow flange beams, *Thin-Walled Structures*, Volume 119, 2017, Pages 499-509, <https://doi.org/10.1016/j.tws.2017.05.033>.
- (9) Li, Z., Leng, J., Guest, J. K., & Schafer, B. W. (2016). Two-level optimization for a new family of cold-formed steel lipped channel sections against local and distortional buckling. *Thin-Walled Structures*, 108, 64–74. <https://doi.org/10.1016/j.tws.2016.07.004>.
- (10) Tran, T., & Li, L. yuan. (2006). Global optimization of cold-formed steel channel sections. *Thin-Walled Structures*, 44(4), 399–406. <https://doi.org/10.1016/j.tws.2006.04.007>.
- (11) Magnucki, K., Maćkiewicz, M., & Lewiński, J. (2006). Optimal design of a mono-symmetrical open cross section of a cold-formed beam with sinusoidally corrugated flanges. *Thin-Walled Structures*, 44(5), 554–562. <https://doi.org/10.1016/j.tws.2006.04.016>.
- (12) Pala, M., & Caglar, N. (2007). A parametric study for distortional buckling stress on cold-formed steel using a neural network. *Journal of Constructional Steel Research*, 63(5), 686–691. <https://doi.org/10.1016/j.jcsr.2006.07.005>.
- (13) Wan, H. X., & Mahendran, M. (2015). Behaviour and strength of hollow flange channel sections under torsion and bending. *Thin-Walled Structures*, 94, 612–623. <https://doi.org/10.1016/j.tws.2015.05.013>.
- (14) Ayhan, D., & Schafer, B. W. (2015). Cold-formed steel member bending stiffness prediction. *Journal of Constructional Steel Research*, 115, 148–159. <https://doi.org/10.1016/j.jcsr.2015.07.004>.
- (15) Anbarasu, M., & Ashraf, M. (2017). Interaction of local-flexural buckling for cold-formed lean duplex stainless steel hollow columns. *Thin-Walled Structures*, 112, 20–30. <https://doi.org/10.1016/j.tws.2016.12.006>.
- (16) Kurniawan, C. W., & Mahendran, M. (2009). Elastic lateral buckling of simply supported LiteSteel beams subject to transverse loading. *Thin-Walled Structures*, 47(1), 109–119. <https://doi.org/10.1016/j.tws.2008.05.012>.
- (17) Perera, N., & Mahendran, M. (2019). Finite element analysis and design for section moment capacities of hollow flange steel plate girders. *Thin-Walled Structures*, 135, 356–375. <https://doi.org/10.1016/j.tws.2018.10.014>.
- (18) Chen, D. H., & Masuda, K. (2016). Rectangular hollow section in bending: Part I – Cross-sectional flattening deformation. *Thin-Walled Structures*, 106, 495–507. <https://doi.org/10.1016/j.tws.2015.12.019>.
- (19) Hassan, E. M., Serror, M. H., & Mourad, S. A. (2017). Numerical prediction of available rotation capacity of cold-formed steel beams. *Journal of Constructional Steel Research*, 128, 84–98. <https://doi.org/10.1016/j.jcsr.2016.08.010>.
- (20) Siahaan, R., Mahendran, M., & Keerthan, P. (2016). Section moment capacity tests of rivet fastened rectangular hollow flange channel beams. *Journal of Constructional Steel Research*, 125, 252–262. <https://doi.org/10.1016/j.jcsr.2016.06.021>.
- (21) Becque, J., & Rasmussen, K. J. R. (2009). Numerical Investigation of the Interaction of Local and Overall Buckling of Stainless Steel I-Columns. *Journal of Structural Engineering*, 135(11), 1349–1356. [https://doi.org/10.1061/\(ASCE\)ST.1943-541X.0000052](https://doi.org/10.1061/(ASCE)ST.1943-541X.0000052).

- (22) Sadowski, A. J., & Rotter, M. J. (2013). On the relationship between mesh and stress field orientations in linear stability analyses of thin plates and shells. *Finite Elements in Analysis and Design*, 73, 42–54. <https://doi.org/10.1016/j.finel.2013.05.004>.
- (23) Schafer, B. W., Li, Z., & Moen, C. D. (2010). Computational modeling of cold-formed steel. *Thin-Walled Structures*, 48(10–11), 752–762. <https://doi.org/10.1016/j.tws.2010.04.008>.
- (24) Dubina, D., Ungureanu, V., & Landolfo, R. (2013). Design of Cold-formed Steel Structures: Eurocode 3: Design of Steel Structures. Part 1-3 Design of Cold-formed Steel Structures. <https://doi.org/10.1002/9783433602256>.
- (25) Huang, Y., & Young, B. (2013). Experimental and numerical investigation of cold-formed lean duplex stainless steel flexural members. *Thin-Walled Structures*, 73, 216–228. <https://doi.org/10.1016/j.tws.2013.07.019>.
- (26) British Standards Institution. (2005). Eurocode 3: Design of steel structures. London: BSI.
- (27) Camotim, D., Silvestre, N., Gonçalves, R., & Dinis, P. B. (2006). GBT-based Structural Analysis of Thin-walled members: Overview, Recent Progress and Future Developments. In M. Pandey, W.-C. Xie, & L. Xu (Eds.), *Advances in Engineering Structures, Mechanics & Construction* (Vol. 140, pp. 187–204). Springer Netherlands. https://doi.org/10.1007/1-4020-4891-2_16.
- (28) Dassault Systèmes. (2016). Abaqus 2016 Documentation. © Dassault Systemes.
- (29) Lee, J., Kim, S. M., & Seon Park, H. (2006). Optimum design of cold-formed steel columns by using micro genetic algorithms. *Thin-Walled Structures*, 44(9), 952–960. <https://doi.org/10.1016/j.tws.2006.08.021>.